



# Functionalization of Biomass-derived Activated Carbon and Electrochemical Reduction for the Recovery of Gold from Mobile Phone Leachate

Mochamad Lutfi Firmansyah<sup>1</sup> · Ilma Amalina<sup>1</sup> · Intan Nurul Rizki<sup>1</sup> · Asmaul Mashad Alfaza<sup>1</sup> · Prastika Krisma Jiwanti<sup>1</sup> · Aishah Abdul Jalil<sup>2,3</sup> · Masahiro Goto<sup>4,5</sup>

Received: 23 April 2023 / Accepted: 19 September 2023 / Published online: 20 October 2023  
© The Author(s) 2023

## Abstract

In this age of cutting-edge technology, electronic equipment consumption, such as mobile phones, has increased tremendously. This was followed by a staggering increase in electronic waste (e-waste). However, it has been known that e-wastes contain higher amounts of precious metals than pristine sources, such as Au, which is valuable as an alternative precious metal source. Due to its various advantages, adsorption has emerged as one of the most common metal removal or recovery methods. A crucial aspect of adsorption is developing a cost-effective adsorbent for selective recovery of Au from the e-wastes. Thus, functionalized biomass-based adsorbent was developed to recover precious metals from e-waste. Functionalized activated carbon (ACIL900) has an appealing high adsorption capacity ( $116.2 \text{ mg g}^{-1}$ ) performance and follows the chemisorption route, which fits with the monolayer model. The presence of IL boosts the adsorption efficiency due to its compatible interaction with the metal complexes. Remarkably, ACIL900 could quantitatively adsorb precious metals and several base metals from mobile phone leachate. The selective recovery of Au from the adsorbent was performed by sequential desorption using various solutions. Finally, Au was successfully recovered from the desorption solution using an electrochemical reduction process. ACIL900 was also found to maintain its performance for three adsorption–desorption cycles. This work reported the full recovery of Au from e-waste to its final pure product through the combination of adsorption, sequential desorption, and electrochemical reduction.

**Keywords** Activated carbon · Ionic liquid · Gold · Electronic waste · Waste recycling

## 1 Introduction

Technology has driven changes in almost every sector of human life over the past few decades, as evidenced by the incredible increases in performance, a significant reduction in consumer prices, and extensive choices in people's daily electric appliances. However, the obsolescence of modern appliances becomes a significant issue due to the short lifespan of electrical equipment usage of 3–5 years [1]. The modern world has generated electronic waste (e-waste) at an alarming rate resulting in a 30% increase in e-wastes production between 2014–2030 [2]. However, in most developing countries, especially Indonesia, e-wastes need to be regulated because several studies have predicted that the number of e-wastes products in Indonesia will double in the next decade [3]. Mairizal et al. (2021) have estimated that Indonesia's per capita e-wastes production will increase by 30% in 2040 [4]. It is unfortunate that without proper regulation and

✉ Mochamad Lutfi Firmansyah  
ml.firmansyah@ftmm.unair.ac.id

<sup>1</sup> Nanotechnology Engineering, Faculty of Advanced Technology and Multidisciplinary, Airlangga University, Jl. Dr. Ir. H. Soekarno, Surabaya 60115, Indonesia

<sup>2</sup> Centre of Hydrogen Energy, Institute of Future Energy, Universiti Teknologi Malaysia, UTM Johor Bahru, 81310 Johor, Malaysia

<sup>3</sup> Faculty of Chemical and Energy Engineering, Universiti Teknologi Malaysia, UTM Johor Bahru, 81310 Johor, Malaysia

<sup>4</sup> Department of Applied Chemistry, Graduate School of Engineering, Kyushu University, 744 Motooka, Nishi-Ku, Fukuoka 819-0395, Japan

<sup>5</sup> Center for Future Chemistry, Kyushu University, 744 Motooka, Nishi-Ku, Fukuoka, Japan



management implementation, e-wastes will significantly be a threat to the Indonesian environment and health. On the bright side, recycling e-wastes also brings benefits not only to the environmental sector but also to the economic sector. It is estimated that e-wastes from mobile phones contain significantly higher levels of precious metals than metals from natural sources. Global e-wastes (2019) were estimated to contain 320 tonnes of precious metals with a valuation of over 13 billion USD, with gold being the most significant contributor (200 kt, 9 billion USD) [5]. As scholars and researchers have observed in recent years, the dependency on resources from several countries can be a significant obstacle. South Africa and Russia currently account for more than 75% of the global supply of platinum, palladium, and rhodium [6]. E-waste recycling may help reduce reliance on some of the world's most critical resource-producing countries.

Regarding the recycling process, mechanical dismantling and separation in e-waste are typically the first steps in the recycling process, followed by a hydrometallurgical or bio-metallurgical process [7]. Solvent extraction, precipitation, electrolysis, cementation, and adsorption can separate and purify metals from e-wastes leachate. Among these processes, the adsorption process is known to have financial and practical advantages by providing an economical and sustainable opportunity for recovering precious metals from e-wastes because it can be efficiently done by developing adsorbents to recover precious metals, like gold, platinum, and palladium. Several adsorbents, including graphene oxide, mesoporous silica, alumina, and membrane matrix, have shown an excellent affinity toward Au [8]. The interest in converting palm oil agro-industry biomass into a value-added product has steadily increased. Various methods have been employed to convert biomass (e.g., composting, pelletizing, briquetting, pyrolysis, and enzymatic digestion). Activated carbon (AC) is a highly desired product due to its versatility [9]. Nonetheless, palm oil agro-industry biomass, such as palm kernel shell (PKS), still needs to be fully exploited in Indonesia due to its massive amount, leading to difficulty handling and transporting. PKS is a good precursor for AC production. The performance of AC derived from PKS was demonstrated in studies evaluating its adsorption of heavy metals and other pollutants [10–12].

Several approaches have been studied previously to enhance the adsorption capacity of activated carbon. Kharrazi et al. (2020) and Macias-Garcia et al. (2017) reported physical modification of AC through heat treatment [13, 14]. The modification significantly increased the adsorption capacity toward transition metals due to changes in AC surface properties. Surface functionalization, acid modification, and active agent immobilization have been carried out to modify the properties of AC chemically. Lesaoana et al. (2019) explored the acid modification of AC using  $\text{HNO}_3$  and  $\text{H}_2\text{SO}_4$ , which increased surface properties and adsorption capacity [15].

Nadeem et al. (2006) and Rehman et al. (2019) reported the modification through impregnation resulting in an enhancement in physicochemical properties leading to an increase in the adsorption capacity of AC [16, 17]. One of these modifications is grafting ionic liquids (IL) to improve the adsorbent capability. IL has been tested as an electrolyte, chemical capture technology, bacterial sensing, solvent, and metal extraction [18–21]. However, IL has a significant drawback due to its high viscosity, which leads to using a large amount of volatile organic compounds (VOCs). However, this disadvantage could be addressed by grafting the IL onto a solid support, which reduces their viscosity issue. An initial report was working on the IL functionalized mesoporous silica adsorbent as the solid support for recovering Pt and Pd [22]. Similar works were also reported by Kumar et al. (2015) and Sharma et al. (2016), who highlighted the use of the impregnation method over grafting for Pd(II) recovery [23, 24]. When this article was written, there were few reports on recovering Au from an actual mobile phone leachate using palm biomass as an adsorbent. Hence, this work attempted to explore the potential of the palm biomass-derived and IL-enhanced activated carbon as an adsorbent to recover Au from the mobile phone leachate selectively. This report also investigated the adsorption behavior of Au in the batch adsorption process, covering kinetic, thermodynamic, and isotherm. Afterward, the selective separation of Au was conducted by sequential desorption and Au recovery from the desorption solution through electrochemical reduction.

## 2 Materials and Methods

### 2.1 Materials

The palm kernel shell (PKS) was obtained from Tricitra Agri Perdana Inc., Bogor. Standard solution of Au(III) ( $1000 \text{ mg L}^{-1}$  in  $1 \text{ mol L}^{-1}$  HCl), dimethyl ether ( $\geq 95\%$ ) 1-methylimidazole, and 3-(chloropropyl)trimethoxy silane were purchased from Sigma-Aldrich. Dichloromethane ( $\geq 95\%$ ),  $\text{Na}_2\text{SO}_3$ , KOH, NaOH,  $\text{NH}_4\text{OH}$ ,  $5 \text{ mol L}^{-1}$   $\text{H}_2\text{SO}_4$ ,  $5 \text{ mol L}^{-1}$  HCl, and  $5 \text{ mol L}^{-1}$   $\text{HNO}_3$  were purchased from Merck.  $\text{CS}(\text{NH}_2)_2$ ,  $\text{Na}_2\text{S}_2\text{O}_3$ , and  $\text{NaClO}_4$  were purchased from Loba Chemie. All reagents were of analytical grade, and the necessary solutions were prepared in aquadest.

### 2.2 Pretreatment and Activation of Activated Carbon

The PKS was washed, dried overnight at 383 K, and ground using an electrical grinder (Q2-8050, China). After that, a mechanical grinder (Timemore Chestnut C2, Thailand) was used to pulverize PKS, and the size separation was done using a mesh strainer and a sieve shaker. Then, the carbonization

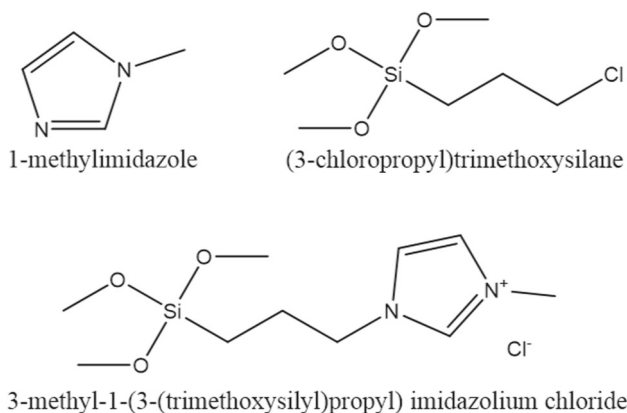


**Fig. 1** Chemical structure of the IL and its precursor

process was performed using a muffle furnace (Nabertherm L 9/11/SKM, Germany) for two h at 973 K. Furthermore, the carbonized samples were soaked in 0.1 g mL<sup>-1</sup> KOH solution with a ratio of 4:1 for 24 h. Carbonization was generated under an N<sub>2</sub> atmosphere at 1173 K. The final product was denoted as AC900 and washed thoroughly using 0.1 mol L<sup>-1</sup> HCl and distilled water until it reached a pH of 7. Finally, AC900 was air-dried overnight in an oven at 383 K.

### 2.3 Functionalization of Activated Carbon

The synthesis of 3-methyl-1-(3-(trimethoxysilyl)propyl)imidazolium chloride was adapted from the works of Zhang et al. (2009) and Lievano and Diaz (2016) [25, 26]. The IL was prepared through an alkylation reaction between 1-methylimidazole and (3-chloropropyl)trimethoxysilane in a 1:1.5 ratio. The mixture was constantly stirred for 18 h at 368 K under reflux conditions, followed by purification using dimethyl ether in a rotary evaporator. The structure of the IL and its precursor is presented in Fig. 1. Then, the final product was characterized using <sup>13</sup>C nuclear magnetic resonance (NMR). To immobilize IL onto AC900, IL was diluted four times using toluene, then mixed with AC900 in a 1:5 solution in a round-bottom flask under an N<sub>2</sub> atmosphere at 363 K for 20 h. Subsequently, the unreacted organic compound was extracted using dichloromethane, and the purification using a rotary evaporator yielded the final product, a solid functionalized AC900, denoted as ACIL900.

The physical properties of ACIL900 were characterized using X-ray diffraction (XRD, MiniFlex, Rigaku, Tokyo, Japan), scanning electron microscopy (SEM, Phenom Desktop ProXL, Thermo Fisher Scientific Inc., USA), and gas adsorption (Beckman Coulter SA3100, USA). ACIL900 chemical properties were characterized using NMR (JNM-ECZ500, Jeol Ltd., Tokyo, Japan) and a Fourier transform-infrared spectrophotometer (FTIR, Thermo Nicolet Avatar 360, Thermo Fisher Scientific Inc., USA).

### 2.4 Preparation of Mobile Phone Leachate

The processing and leaching of the discarded mobile phone were kindly done by Shibata Industry Co. Ltd. (Japan). A mechanical milling process of the discarded phone into a powder with  $\geq 2$  mm diameter was conducted using a rotary cutter, followed by metal separation from the powder physically using a magnetic force. Then, the remaining PCBs were removed from the powder through calcination, and the digestion of the powdered mobile phone was carried out by Matsuda Sangyo (Japan). The final product was subsequently digested in aqua regia, denitrated, and concentration adjusted to 4 mol L<sup>-1</sup> with HCl.

### 2.5 Adsorption Procedure

The Au(III) adsorption behavior was initially investigated in a synthetic solution. Then, a batch adsorption–desorption process was carried out to recover Au(III) from mobile phone leachate. The adsorption process was carried out by mixing 200 g of ACIL900 and Au(III) (100 mg L<sup>-1</sup>) for a set period with three replications. The mixture was shaken using a linear shaker (DLAB SK-L180-E) at 160 rpm at room temperature. The concentration of the metals in the mobile phone leachate used in this study was adjusted by diluting the original leachate. The concentration of Au(III) was measured by atomic absorption spectroscopy (PerkinElmer PinAAcle 900 T) and determined by using Eq. (1). Furthermore, the adsorption behavior of ACIL900 toward precious metals was determined using Langmuir (Eq. (2)) and Temkin (Eq. (3)) isotherm models; pseudo-first (Eq. (4)) and pseudo-second rate order (Eq. (5)) kinetic models:

$$q_{eq} = \left( \frac{C_i - C_{eq}}{W} \right) x V \quad (1)$$

$$\frac{1}{q_{eq}} = \frac{1}{q_o} + \frac{1}{q_o K_L} \frac{1}{C_{eq}} \quad (2)$$

$$q_{eq} = \frac{RT}{b_T} \ln A_T + \frac{RT}{b_T} \ln C_{eq} \quad (3)$$

$$\log(q_{eq} - q_t) = \log q_{eq} - K_1 t \quad (4)$$

$$\frac{t}{q_t} = \frac{1}{K_2 q_{eq}^2} + \frac{1}{q_{eq}} t \quad (5)$$

The amount of Au(III) adsorbed at equilibrium was  $q_{eq}$ . The constants of the Langmuir, Temkin isotherm model, pseudo-first-order, and pseudo-second-order kinetic model were represented by  $K_L$  (L mg<sup>-1</sup>),  $b_T$  (kJ mol<sup>-1</sup>),  $K_1$ , and  $K_2$ , respectively. The adsorption capacity was represented by  $q_o$  (mg g<sup>-1</sup>). In addition, the equilibrium binding constant was presented as  $A_T$  (L mol<sup>-1</sup>).



In the desorption experiment, 50 mL of various desorption solutions of  $\text{H}_2\text{SO}_4$ ,  $\text{NH}_4\text{OH}$ ,  $\text{Na}_2\text{SO}_3$ ,  $\text{Na}_2\text{S}_2\text{O}_3$ ,  $\text{CS}(\text{NH}_2)_2$ , and  $\text{NaClO}_4$  were mixed with the used ACIL900 and constantly mixed for 8 h. The mixture was then separated by filtration, and the metal concentration in the desorption solution was measured using AAS. The desorption experiment was conducted in triplicate. The desorption efficiency ( $D\%$ ) was calculated as presented in Eq. (6).

$$D\% = \frac{C_d \times V \times Q_d}{W \times Q_e} \times 100 \quad (6)$$

where  $V$ ,  $C_d$ , and  $W$  are the desorption solution volume (L), metal ion concentration of desorption solution ( $\text{mg L}^{-1}$ ), and mass of ACIL900 (g), respectively.

## 2.6 Electrochemical Reduction of Au(III)

The electrochemical reduction was conducted in a one-compartment cell. The electrodes used were Cu as a working electrode, Pt spiral, and Ag/AgCl as a counter and a reference electrode. The Cu and Pt electrodes were pre-treated by ultrasonication in ultrapure water. A Cu electrode with a surface area of  $2.54 \text{ cm}^2$ , an Ag/AgCl electrode, and the Pt spiral electrode were immersed in the Au desorption solution cell (5 mL). The Au reduction was carried out for 100 s using the chronoamperometry technique with a reduction potential of  $-0.2 \text{ V}$  (vs. Ag/AgCl). The reduced Au nanoparticles would be deposited on the Cu electrode.

## 3 Results and Discussion

### 3.1 Physicochemical Characterization of ACIL900

The ACIL900 adsorbent showed an irregular grain morphology (Fig. 2A), unaffected by the grafting process. The EDX spectra of ACIL900 presented Si and N elements originating from the IL (Fig. 2B). The elemental mapping in subsequent processes showed a uniform distribution of Si and N originating from the IL, which could indicate the success of IL grafting onto ACIL900. The diffractogram of ACIL900 shows a maximum of  $23^\circ$  (Fig. 2C), which could be associated with the crystal face index of 002, similarly observed in graphite [27]. The crystal face index of 002 was due to the presence of graphitic crystallite layers. The resulting AC

created a multi-layer graphitic crystallite at a high pyrolysis temperature.

Figure 2D and Table 1 show ACIL900  $\text{N}_2$  adsorption behavior and pore size distribution. The  $\text{N}_2$  adsorption isotherm by ACIL900 shows a type IV isotherm with an  $\text{H}_3$  hysteresis loop. These results indicate the presence of mesopores in the form of interparticle porosity originating from the amorphous structure of activated carbon [28]. In line with the isotherm result, the presence of mesopore only accounted for less than 20% of the total pore volume. Moreover, it was demonstrated that the grafting of IL decreased the surface area and the porosity volume by less than 10%. The grafting of IL could induce a pore blockage of the AC, which reduces the AC surface properties. The decrease in the pore volume was more apparent in the micropore than in the mesopore, indicating that IL was mainly deposited within the microporous structure.

The surface functional groups on ACIL900 were identified with FTIR (Fig. 2E). A broad adsorption band at  $3400 \text{ cm}^{-1}$  was associated with the stretching vibration of the O–H groups, which may have been caused by moisture during the measurement stage. The absorption bands of silica-related peaks were observed in ACIL900 at 790, 1070, and  $1181 \text{ cm}^{-1}$ , which is related to the vibration of Si–C and Si–O– $\text{CH}_3$ , respectively [29]. In addition, the presence of C = N originating from the IL was detected in the adsorbent by the absorption band at  $1690 \text{ cm}^{-1}$  [30].

Moreover, the imidazolium ring of the IL in the ACIL900 was presented by the absorption band at  $1278 \text{ cm}^{-1}$  [30]. Due to the aliphatic chain in the IL, there is a significant difference in the absorption bands at  $2920\text{--}2840 \text{ cm}^{-1}$  than that of AC. In the spectrum, absorption bands were also observed in 1615 and  $1715 \text{ cm}^{-1}$ , attributed to the stretching vibration of C = C and C = O and conjugated C = O from the activated carbon, respectively. Moreover, the adsorption bands at 1660 and  $1030 \text{ cm}^{-1}$ , observed in the pre-grafted AC, were associated with the C–O stretching vibration [31].

### 3.2 Adsorption Behavior of Au(III)

Langmuir and Temkin isotherm models were used to determine the adsorption behavior of Au(III), in which both model's linear fit are presented in Fig. 3A and B, respectively. The adsorption of Au(III) was found compatible with both models, as evidenced by the high correlation factor ( $R^2$ )

**Table 1** Surface properties of the ACIL adsorbent

Catalyst	Surface area [ $\text{m}^2 \text{ g}^{-1}$ ]	Microp. Volume [ $\text{cm}^3 \text{ g}^{-1}$ ]	Mesop. Volume [ $\text{cm}^3 \text{ g}^{-1}$ ]	Total Volume [ $\text{cm}^3 \text{ g}^{-1}$ ]
ACIL900	661.5	0.2760	0.0568	0.3321
AC	735.1	0.2926	0.0791	0.3657



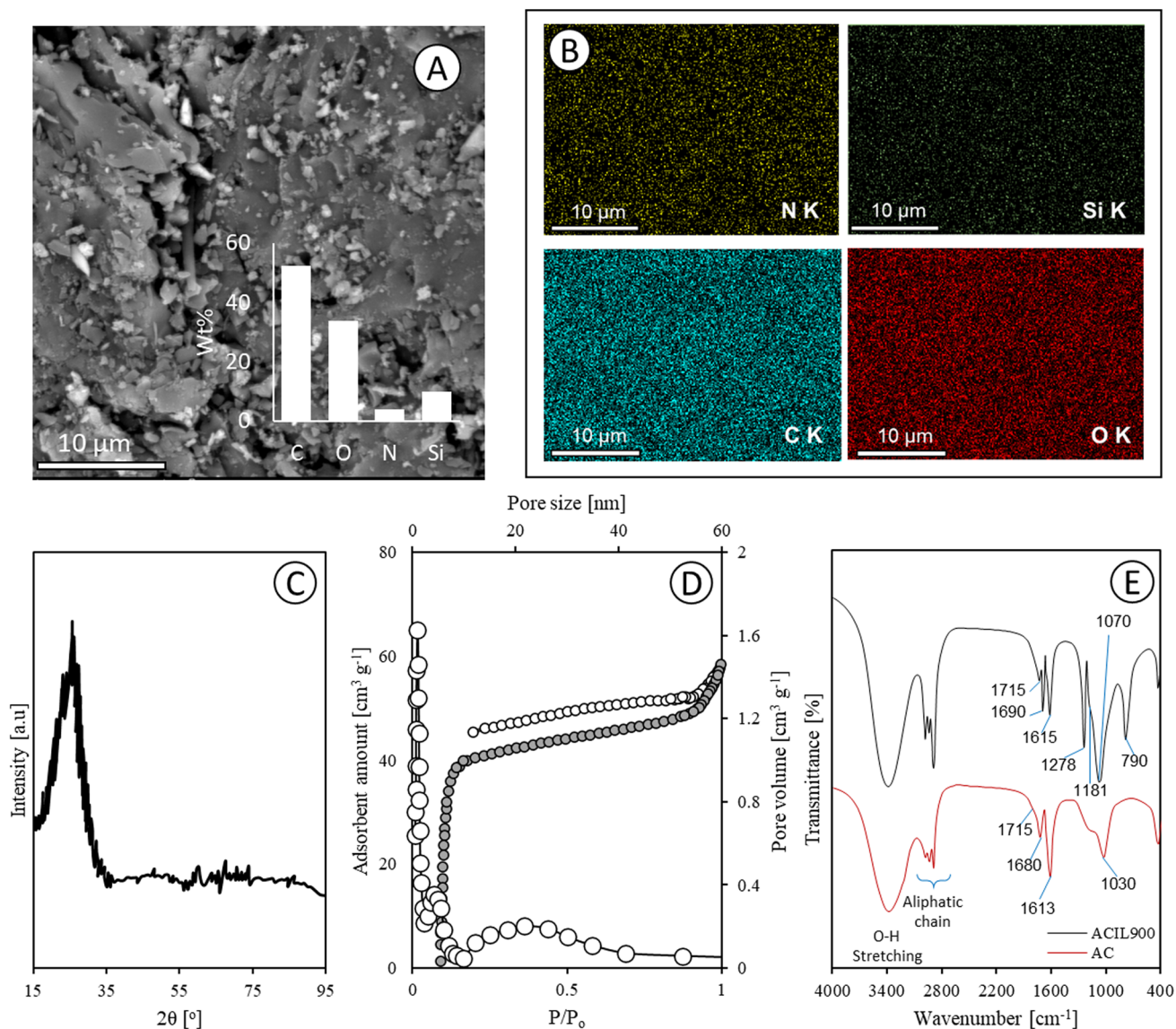


**Fig. 2** Physicochemical characterization of ACIL900 **A** SEM images, **B** elemental mapping, **C** Diffractogram, **D** adsorption isotherm of N<sub>2</sub> and pore size distribution, and **E** FTIR spectrum

**Table 2** Thermodynamic parameter of Au(III) adsorption by ACIL900

T (K)	ΔG [kJ mol <sup>-1</sup> ]	ΔH [kJ mol <sup>-1</sup> ]	ΔS [J mol <sup>-1</sup> K <sup>-1</sup> ]
298	- 29.88		
303	- 29.84		
308	- 29.75	- 32.37	- 8.36
318	- 29.71		
328	- 29.67		

value. As for observation, the parameters of each model are presented in Table 2. At various concentrations, ACIL900 maintained an adsorption efficiency of 98% up to 300 mg L<sup>-1</sup> and exhibited a high adsorption capacity of 116.2 mg g<sup>-1</sup>.

The value of the Langmuir constant was close to unity (0.86 L mol<sup>-1</sup>), which indicated the favorable interaction between the adsorbate and adsorbent [32]. The Temkin isotherm showed a positive slope indicating that the Au(III) adsorption was an exothermic process. In particular, the Temkin constant (*b<sub>T</sub>*) obtained from the model referred to a value of 68.5 kJ mol<sup>-1</sup>, which indicated that Au(III) was chemically adsorbed onto ACIL900 [33]. The chemical adsorption process of Au(III) may occur through ion exchange between [AuCl<sub>4</sub>]<sup>-</sup> and the anionic moieties of IL.

The thermodynamic properties of Au(III) adsorption were determined from the experimental data in the temperature range of 298–328 K using a linearized Van't Hoff equation [34]:

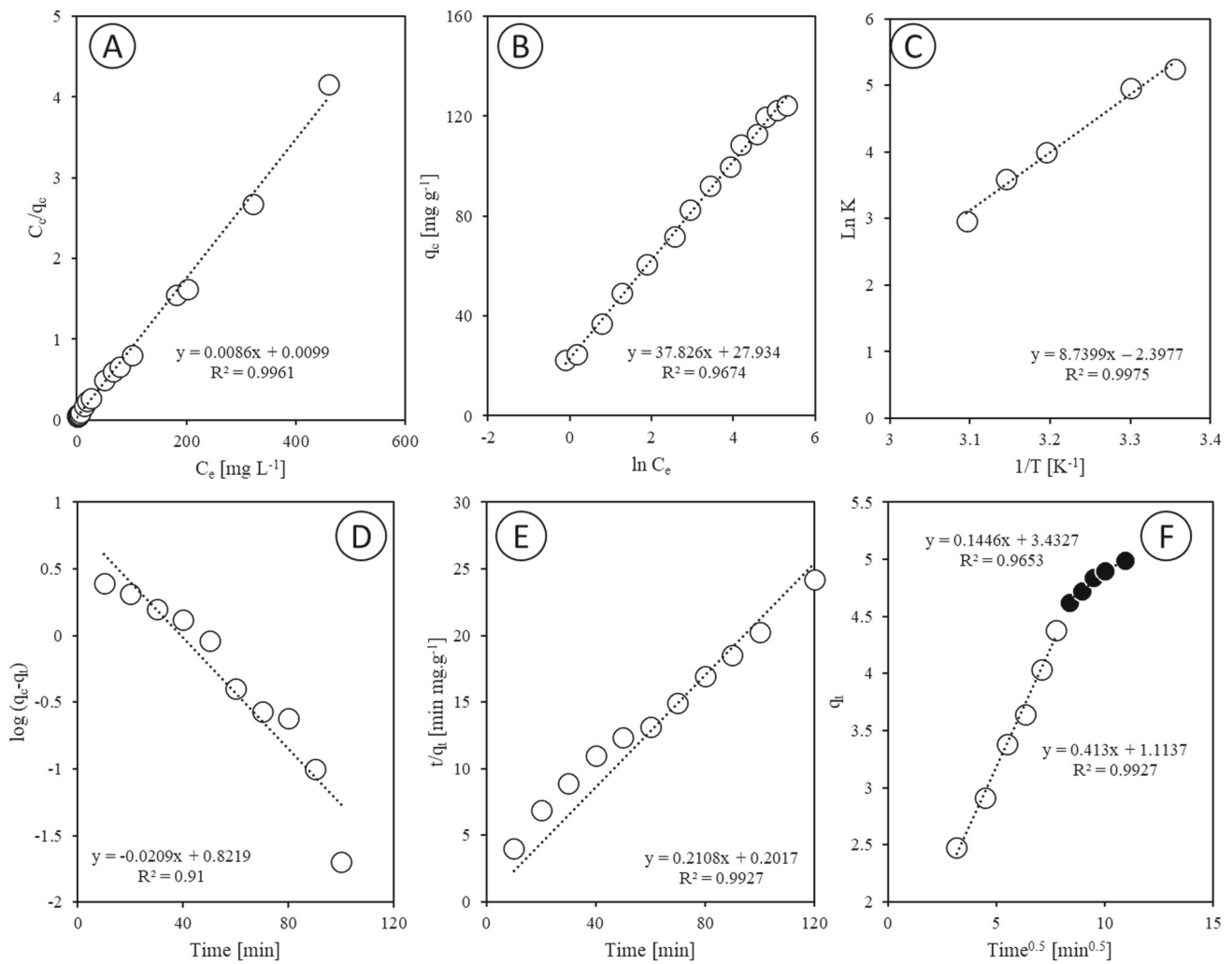


**Fig. 3** Linear fit of **A** Langmuir isotherm model, **B** Temkin isotherm model, **C** Van't Hoff model, **D** pseudo-first-order kinetic, **E** pseudo-second-order kinetic model, and **F** intraparticle diffusion model of Au(III) adsorption by ACIL900

$$\ln K_D = -\frac{\Delta H}{R} \left( \frac{1}{T} \right) + \frac{\Delta S}{R} \quad (7)$$

The linear plot between  $\ln(q_{eq}/C_{eq})$  and  $C_{eq}$  at various temperatures determined the equilibrium constant ( $K_D$ ). Then, the linear equation from the plot between  $\ln K_D$  vs.  $1/T$  provides the values of Gibbs free energy ( $\Delta G$ ,  $\text{kJ mol}^{-1}$ ), enthalpy ( $\Delta H$ ,  $\text{kJ mol}^{-1}$ ), and entropy ( $\Delta S$ ,  $\text{J mol}^{-1} \text{K}^{-1}$ ).

The increase in temperature resulting in a decrease in the adsorption of Au(III) (Fig. 3C) and demonstrated negative  $\Delta H$ , positive  $\Delta S$ , and negative  $\Delta G$  value (Table 2), indicating that the reaction occurred exothermically and spontaneously with a high affinity for Au(III) [35]. Moreover, the linearized Arrhenius equation (Eq. 8) could be used to determine both the  $E_a$  and the adsorption rate as follows:

$$\ln K_t = \ln \frac{q_{eq}}{C_{eq}} = \ln A - \frac{E_a}{RT} \quad (8)$$

and the  $E_a$  value obtained of Au(III) adsorption was  $85.4 \text{ kJ mol}^{-1}$ . It was noted that the Au(III) adsorption followed a chemisorption pathway because the  $E_a$  value was higher than that of  $40 \text{ kJ mol}^{-1}$ , which was in line with the Temkin isotherm model [36].

The kinetic study of the Au(III) adsorption was performed within 10–90 min, while ACIL900 could reach equilibrium within 60 min. The kinetic behavior was determined using the pseudo-first-order and pseudo-second-order kinetic models [37]. The closeness of  $q_e$  value between the calculation and experimental (Table 3) and the value of  $R^2$  (Fig. 3D and E) reflected the better fit of the adsorption of Au(III) with the pseudo-second-order kinetic model. These results made it possible to conclude that the Au(III) adsorption by ACIL900 followed the pseudo-second-order kinetic model by a chemical adsorption pathway. However, these results cannot explain the rate-limiting step of the adsorption

**Table 3** Kinetic parameter of Au(III) adsorption by ACIL900

Kinetic model	Parameters	Adsorbent	
		Chitosan	Chi_IL
Pseudo-first order	$K_1$	0.041	0.054
	$q_{e,exp}$	12.31	12.45
	$q_{e,cal}$	8.99	7.68
	$R^2$	0.9480	0.9967
Pseudo-second order	$K_2$	0.072	0.092
	$q_{e,exp}$	12.31	12.45
	$q_{e,cal}$	12.26	12.43
	$R^2$	0.9995	0.9999

process. The Au(III) adsorption rate could be limited by surface adsorption (boundary layer) or intraparticle diffusion. As a consequence, the Weber–Morris intraparticle diffusion model (Eq. (9)) was used to explain this issue [38]:

$$q_t = K_{diff}t^{0.5} + C \quad (9)$$

where  $q_t$  ( $\text{mg g}^{-1}$ ) and  $K_{diff}$  ( $\text{mg g}^{-1} \text{min}^{-0.5}$ ) represented the metal adsorption at a specific time and the intraparticle diffusion rate constant by a linear relationship between  $q_t$  and  $t^{0.5}$ . The intercept of the plot,  $C$ , represents the surface adsorption, and its effect was proportional to the intercept value. Two linear graphs were observed in the intraparticle diffusion model, indicating that different rate-limiting steps controlled the Au(III) adsorption. Two different diffusion constants ( $K_{diff,1} = 0.413 \text{ mg g}^{-1}$  and  $K_{diff,2} = 0.144 \text{ mg g}^{-1}$ ) were obtained from the plot due to two linear phases (Fig. 3F). According to Plazinski and Rudzinski (2009), surface adsorption plays a more significant role in the latter part of the adsorption process. This study shows that the first phase intercept was higher than the second phase [39]. In the first phase, the intraparticle mobility of Au(III) becomes more visible until the intraparticle adsorption site is saturated. The surface adsorption process then continued until it was saturated.

### 3.3 Adsorption of Au(III) from Mobile Phone Leachate

The precious metal ions concentrations in the mobile phone leachate are listed in Table 4. The presence of precious metals in mobile phone leachate containing Au ( $160 \text{ mg L}^{-1}$ ), Pt ( $11 \text{ mg L}^{-1}$ ), and Pd ( $7 \text{ mg L}^{-1}$ ). Aside from the precious metals, significantly higher concentrations of various other base metals were also present in the leachate.

The Au adsorption from the mobile phone leachate was carried out in various pH and Cl concentrations. During the pH variation experiment, the Cl concentration of the solution

**Table 4** Elemental composition of the mobile phone leachate

Element	Concentration [ $\text{mg L}^{-1}$ ]
Au	160
Pt	12
Pd	7
Fe	6300
Cu	60,000
Zn	3000
Al	5000
Ni	3200
Pb	30

was maintained at  $4 \text{ mol L}^{-1}$  by adding NaCl solution. It was measured that in the pH variation study, some precious metals, including Pt, Pd, and Au, showed excellent adsorption efficiency (Fig. 4A) yet were recorded to decrease significantly at the pH of 5. Whereas the experiment with the high concentration of Cl<sup>-</sup>, the dominant chlorocomplexes species of Au, Pt, and Pd were  $[\text{AuCl}_4]^-$ ,  $[\text{PtCl}_6]^{2-}$ , and  $[\text{PdCl}_4]^{2-}$ , respectively [40]. This high adsorption efficiency was due to the compatibility between the chlorocomplexes and IL, which allowed the anionic exchange to occur (Fig. 4B). However, it was seen that the ratio of chlorocomplex species changed in the high-pH solution, leading to a decrease in adsorption efficiency. Moreover, it is essential to note that base metals such as Fe, Zn, and Cu were significantly adsorbed, but the adsorption efficiency of these base metals decreased while in the low-pH solution.

Throughout the various concentration of Cl, the adsorption of the precious metals remained constant. However, significant changes were observed in the base metals adsorption efficiency, noting that metal chloride complexes, such as  $[\text{ZnCl}_4]^{2-}$ ,  $[\text{CuCl}_4]^{2-}$ , and  $\text{FeCl}_3$ , were easier to form at high Cl concentrations due to the anion exchange process of IL's anionic moieties [41]. Therefore, to restrict the interference of base metals in the Au(III) adsorption and other precious metals, the further experiment will use a pH of 1 and a Cl concentration of  $1 \text{ mol L}^{-1}$ .

### 3.4 Desorption Studies

Au and other precious metals recovering from the adsorbent was an essential aspect of its practical use since it promotes the adsorbent reusability. As previously discussed, ACIL900 effectively adsorbed precious metals, such as Au ( $157 \text{ mg L}^{-1}$ ), Pt ( $11.8 \text{ mg L}^{-1}$ ), and Pd ( $4 \text{ mg L}^{-1}$ ), as well as several other base metals, such as Zn ( $31.5 \text{ mg L}^{-1}$ ), Cu ( $404 \text{ mg L}^{-1}$ ), and Fe ( $34 \text{ mg L}^{-1}$ ). The desorption efficiency from various desorption solutions of base metals, like Zn(II) and Cu(II), could be quantitatively removed from ACIL900 using

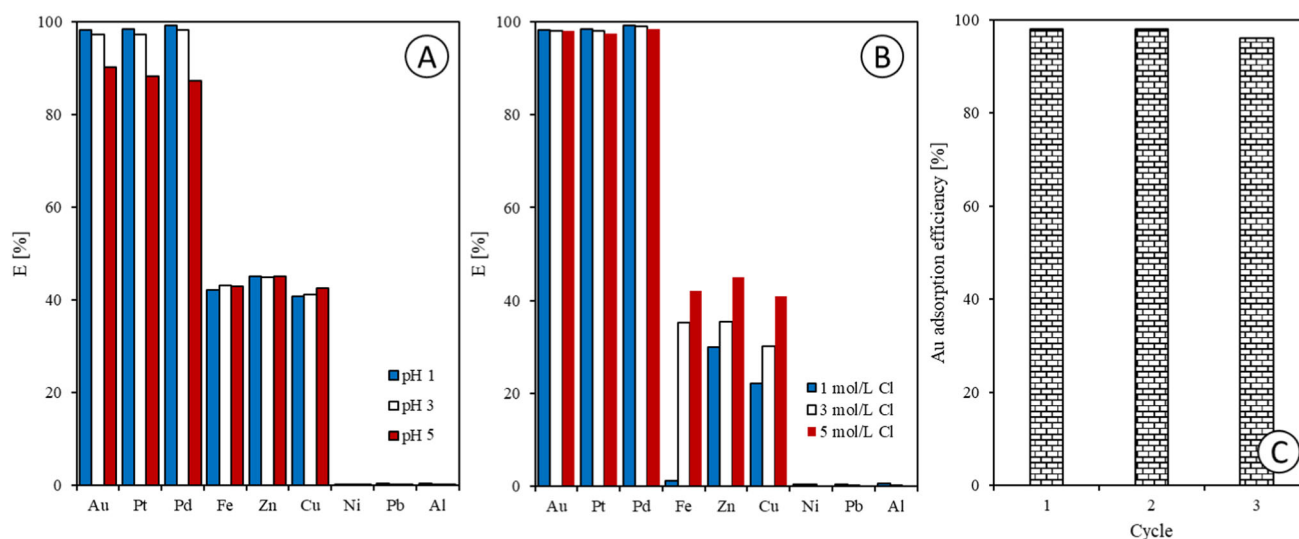


**Fig. 4** The adsorption performance of ACIL900 on the mobile phone leachate in **A** pH variation and **B** Cl concentration; **C** reusability of ACIL900 on the adsorption of Au from mobile phone leachate

**Table 5** Desorption efficiency of various solutions on the adsorbed metals

D [%]	Au(III)	Pt(IV)	Pd(II)	Fe(III)	Zn(II)	Cu(II)
1 mol L <sup>-1</sup> H <sub>2</sub> SO <sub>4</sub>	0	0	0	0	<b>92.7</b>	<b>98.4</b>
5 mol L <sup>-1</sup> H <sub>2</sub> SO <sub>4</sub>	10.2	25.8	14.2	0	<b>88.4</b>	<b>83.2</b>
1 mol L <sup>-1</sup> NH <sub>4</sub> OH	0.2	0.1	15.1	0	<b>98.6</b>	<b>95.5</b>
1 mol L <sup>-1</sup> Na <sub>2</sub> SO <sub>3</sub>	0	0	0	<b>98</b>	0	0
1 mol L <sup>-1</sup> Na <sub>2</sub> S <sub>2</sub> O <sub>3</sub>	<b>99.1</b>	2.1	0.2	0.1	0.2	0
0.1 mol L <sup>-1</sup> CS(NH <sub>2</sub> ) <sub>2</sub>	<b>92.8</b>	15.2	<b>88.6</b>	0	0	0
0.1 mol L <sup>-1</sup> CS(NH <sub>2</sub> ) <sub>2</sub> in 0.1 mol L <sup>-1</sup> HCl	<b>95</b>	6.2	<b>98.2</b>	0.2	0	0
1 mol L <sup>-1</sup> NaClO <sub>4</sub>	0.2	<b>92</b>	42	0	0	0
H <sub>2</sub> O	0	0	0	0	0	0

The bold values shows the highest desorption efficiency of that particular solution

1 mol L<sup>-1</sup> H<sub>2</sub>SO<sub>4</sub> (Table 5). Moreover, the desorption was believed to be due to the formation of ZnSO<sub>4</sub> and CuSO<sub>4</sub> [42], in which high H<sub>2</sub>SO<sub>4</sub> concentration allowed a soluble SO<sub>4</sub> complex formation that led to the removal of the precious metals. Thus, 1 mol L<sup>-1</sup> H<sub>2</sub>SO<sub>4</sub> was chosen to remove Cu and Zn selectively. In comparison, 1 mol L<sup>-1</sup> Na<sub>2</sub>SO<sub>3</sub> was selected to selectively remove Fe metal by the formation of Fe(OH)<sub>2</sub> from the reduction of Fe(III) into Fe(II) [43].

In the desorption of precious metals study, it was noted that precious metals have a strong affinity for Na<sub>2</sub>S<sub>2</sub>O<sub>3</sub>, CS(NH<sub>2</sub>)<sub>2</sub>, and NaClO<sub>4</sub> solutions. However, it was discovered that both CS(NH<sub>2</sub>)<sub>2</sub> and NaClO<sub>4</sub> solutions were shown to be non-selective toward Pt and Pd. Thus, sequential desorption with a different solution could be used to achieve selective desorption of precious metals. The selective recovery of Au by 1 mol L<sup>-1</sup> Na<sub>2</sub>S<sub>2</sub>O<sub>3</sub> was made through the formation of Au(I) and subsequent complexation with (S<sub>2</sub>O<sub>3</sub>)<sup>2-</sup> into [Au(S<sub>2</sub>O<sub>3</sub>)<sub>2</sub>]<sup>3-</sup> ion [44]. In addition, Pd

recovery was conducted using 0.1 mol L<sup>-1</sup> CS(NH<sub>2</sub>)<sub>2</sub> in 0.1 mol L<sup>-1</sup> HCl to minimize the Pt desorption. In this process, the Pd-thiourea complex was formed due to the compatibility between CS(NH<sub>2</sub>)<sub>2</sub> as a soft acid/base and the synergistic effect between CS(NH<sub>2</sub>)<sub>2</sub> and HCl, which promoted the Pd desorption [45]. At last, the Pt removal could be performed using 1 mol L<sup>-1</sup> NaClO<sub>4</sub>, which occurred due to the ion exchange between the chlorocomplexes and [ClO<sub>4</sub>]<sup>-</sup> ion [18].

### 3.5 Reusability

Following these results, Zn, Cu, and Fe were the initial target of sequential desorption using 1 mol L<sup>-1</sup> H<sub>2</sub>SO<sub>4</sub>, and 1 mol L<sup>-1</sup> Na<sub>2</sub>SO<sub>3</sub>, respectively. The selected desorption solution was then used to perform selective recovery of precious metals. At first, Au was recovered selectively using



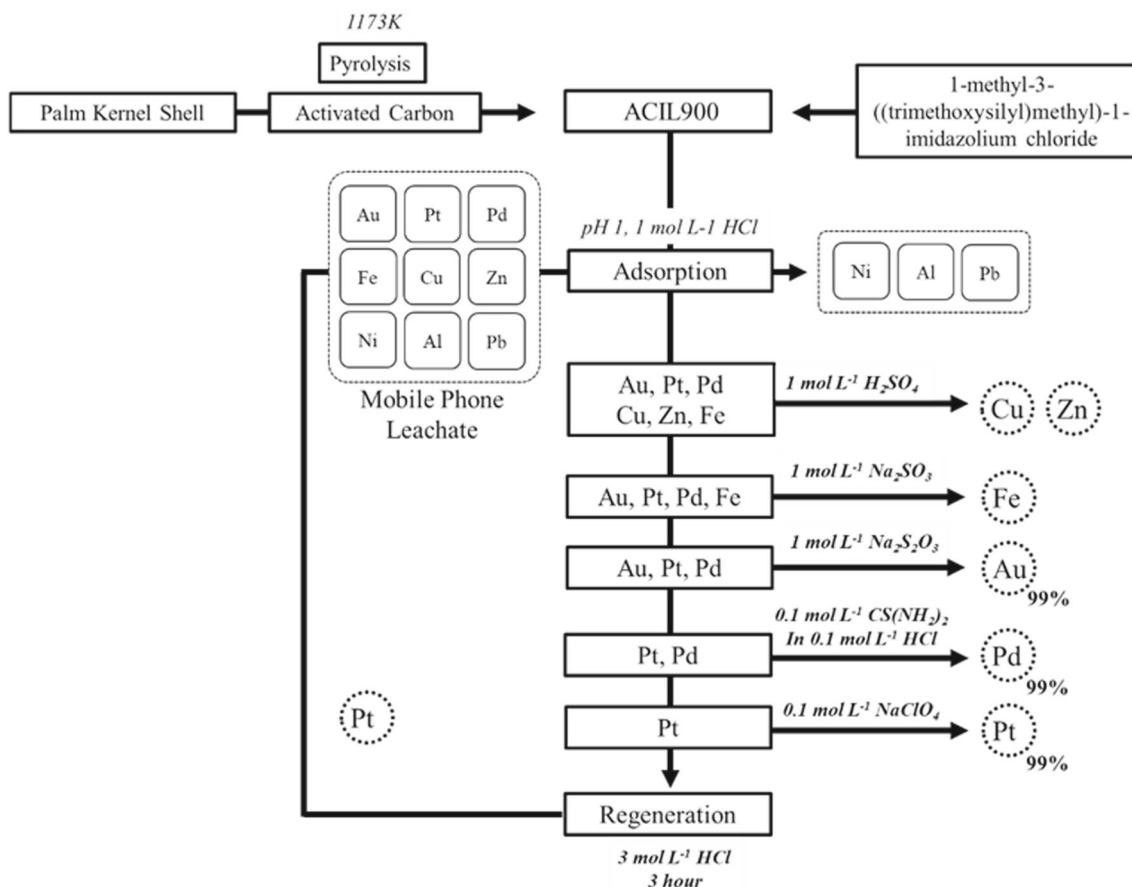


**Fig. 5** Flow chart of the adsorption–desorption cycles of Au from mobile phone leachate using ACIL900

1 mol L<sup>-1</sup> Na<sub>2</sub>S<sub>2</sub>O<sub>3</sub> to remove Au, followed by the desorption of Pd by using 0.1 mol L<sup>-1</sup> CS(NH<sub>2</sub>)<sub>2</sub> in 0.1 mol L<sup>-1</sup> HCl. Finally, Pt was removed from ACIL900 using 1 mol L<sup>-1</sup> NaClO<sub>4</sub>. Before ACIL900 was reused, the adsorbent was treated beforehand with 3 mol L<sup>-1</sup> HCl for 6 h. These adsorption–desorption cycles were completed using the mobile phone leachate, followed by sequential desorption. Following the results in Fig. 4C, it was visible that ACIL900 could be recycled for three cycles without experiencing a significant decrease in function. This suggested that adsorbents could perform long-term adsorption processes. The entire scheme of adsorption–desorption cycles of Au is depicted in Fig. 5.

### 3.6 Electrochemical Reduction of Au

At this stage, the electrochemical reduction method was utilized to recover Au from the desorption solution by depositing the reduced Au onto a copper plate. This step confirmed that the electrodeposited compound consists of Au by a granular morphology, as in Fig. 6A. The diffractogram of the sample, as shown in Fig. 6B, presented diffraction peaks

at 38 and 44°, which indicated the presence of Au with crystal face index of (111) and (200), respectively [46]. Cu<sub>2</sub>O diffraction peaks could be attributed to the electrodeposition plate that comes off while scrapping the electrodeposited Au.

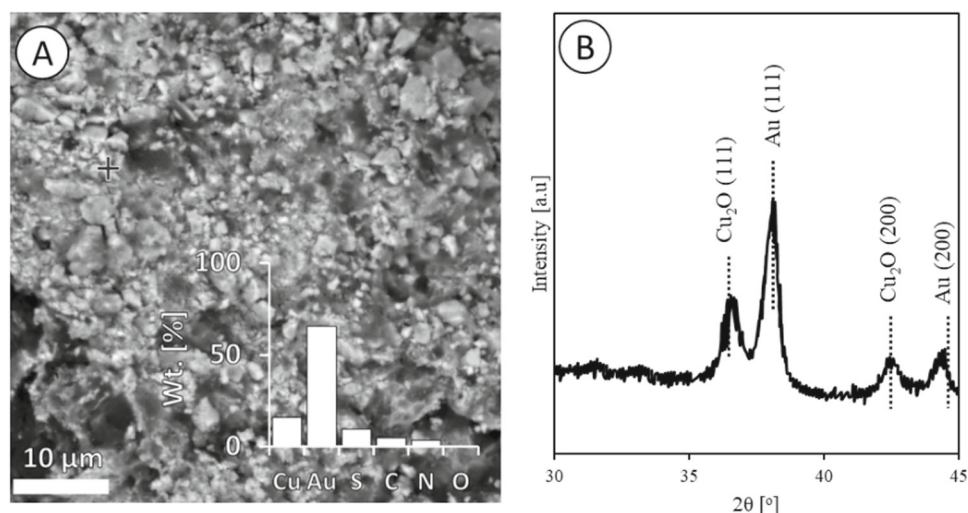
### 3.7 Comparison with the Previous Study

Table 6 compares ACIL900 with a previous study on recovering precious metals from printed circuit boards and mobile phone waste. Precious metal recovery using biomass-derived adsorbent showed comparable performance to the previous study.

## 4 Conclusions

E-waste production has risen significantly due to economic and technological growth in recent decades. However, it turned out that e-wastes were shown to contain much higher amounts of precious metals, such as Au, than pure sources. An adsorption technology was chosen as one of the methods for recovering Au from the mobile phone leachate considering its efficiency for its cost and ease of use.

**Fig. 6** **A** SEM image and EDX analysis and **B** diffractogram of the electrodeposited sample



**Table 6** Comparison between current study and previous works

Sample	Target metal	Methods	Performance	Refs
PCB*	Au, Ag, Bi, Cd, Co, Cr, In, Zn	Pyrolysis, Liquid–liquid Separation	92.2% of Au and 91.3% of Ag were recovered in Cu-rich Substances	[47]
PCB	Au	Thiosulfate Leaching, Electrowinning	75% Au leached and 94% recovery by electrowinning	[48]
PCB	Au, Ag, Pd, Pt, Rh	Smelting, Alloying	95% Au, Ag, Pt, Pd, and Rh recovered in Cu-Fe-Sn alloy	[49]
PCB	Au	Thiourea Leaching, Adsorption	95% Au & 98% Ag recovery with Persimmon tannin gel, and 95% Au and 78% Ag recovery with Activated Charcoal	[50]
PCB	Au	Successive Leaching	85% Au recovery in thiourea leachate	[51]
PCB	Au	Chlorate Leaching, Adsorption	98% Au recovery with Crosslinked Chitosan adsorbent	[52]
MPW**	Au, Cu, Ni	Thiourea Leaching, Adsorption	95% recovery of Au, Cu, and Ni	[53]
MPW	Au	Leaching, Polymeric Membrane	Selective transport of 96% Au into receiving solution	[54]
MPW	Au	Polymeric Membrane	98.83% extraction rate of Au from leachate	[55]
MPW	Au, Pt, Pd	Leaching, Adsorption	99% recovery of Au, Pt, and Pd	This Work

\*Printed Circuit Board

\*\*Mobile Phone Waste

The functionalization of activated carbon (ACIL900) from palm biomass was successfully performed by grafting 1-methyl-3-((trimethoxysilyl)methyl)-1-imidazolium chloride through an alkylation process. The Au adsorption was confirmed to follow a chemical adsorption pathway supported by the isothermal, kinetic, and thermodynamic models. This work noted that ACIL900 showed an adsorption capacity of 116.2 mg g<sup>-1</sup>, and Au was successfully adsorbed from the mobile phone leachate, along with Pt, Pd, Cu, Zn, and Fe. The

selective desorption of these metals was conducted through sequential desorption with different desorption solutions.

To begin with, base metals were removed using 1 mol L<sup>-1</sup> H<sub>2</sub>SO<sub>4</sub> for Cu and Zn and 1 mol L<sup>-1</sup> Na<sub>2</sub>SO<sub>3</sub> for Fe. Meanwhile, selective desorption for precious metals was conducted as follows: 1 mol L<sup>-1</sup> Na<sub>2</sub>S<sub>2</sub>O<sub>3</sub> was used for Au, 0.1 mol L<sup>-1</sup> CS(NH<sub>2</sub>)<sub>2</sub> in 0.1 mol L<sup>-1</sup> HCl for Pd, and 1 mol L<sup>-1</sup> NaClO<sub>4</sub> for Pt. After three cycles of the adsorption–desorption process have experimented with, ACIL900's function and performance remained unimpacted once the

desorption was conducted. The result of this finding was that the recovery of Au from the desorption solution was successfully achieved by using an electrochemical reduction with a reduction potential of  $-0.2$  V into solid Au.

**Author Contributions** MLF carried out funding acquisition, data curation, methodology, investigation, writing—original draft preparation, project administration, supervision, and visualization. IA performed funding acquisition, investigation, methodology, writing, reviewing, and editing. INR carried out data curation, investigation, reviewing and editing, and visualization. AMA performed investigation, and methodology. PKJ carried out data curation, investigation, and writing. AAJ engaged in data curation, supervision, reviewing, and editing. MG engaged in data curation, supervision, reviewing, and editing. All authors read and approved the final manuscript.

**Funding** This work was supported by Badan Pengelola Dana Perkebunan Kelapa Sawit (BPD PKS) Grant Research Scheme 2022 [PRJ-364/DPKS/2022].

**Availability of Data and Materials** All data generated or analyzed during this study are available from the corresponding author on reasonable request.

## Declarations

**Conflict of interest** The authors declare they have no competing interests.

**Open Access** This article is licensed under a Creative Commons Attribution 4.0 International License, which permits use, sharing, adaptation, distribution and reproduction in any medium or format, as long as you give appropriate credit to the original author(s) and the source, provide a link to the Creative Commons licence, and indicate if changes were made. The images or other third party material in this article are included in the article's Creative Commons licence, unless indicated otherwise in a credit line to the material. If material is not included in the article's Creative Commons licence and your intended use is not permitted by statutory regulation or exceeds the permitted use, you will need to obtain permission directly from the copyright holder. To view a copy of this licence, visit <http://creativecommons.org/licenses/by/4.0/>.

## References

- Kastanaki, E.; Giannis, A.: Forecasting quantities of critical raw materials in obsolete feature and smart phones in Greece: a path to circular economy. *J. Environ. Manag.* **307**, 114566 (2022). <https://doi.org/10.1016/j.jenvman.2022.114566>
- Forti, V.; Balde, C.P.; Kuehr, R.; Bel, G.: The Global E-waste Monitor 2020: Quantities, Flows, And The Circular Economy Potential. United Nations University/United Nations Institute for Training and Research, Bonn/Geneva/Rotterdam (2020)
- Kurniawan, K.; Soefihara, M.D.A.; Nababan, D.C.; Kim, S.: Current status of the recycling of e-waste in Indonesia. *Geosyst. Eng.* (2022). <https://doi.org/10.1080/12269328.2022.2142856>
- Mairizal, A.Q.; Sembada, A.Y.; Tse, K.M.; Rhamdhani, M.A.: Electronic waste generation, economic values, distribution map, and possible recycling system in Indonesia. *J. Clean. Prod.* (2021). <https://doi.org/10.1016/j.jclepro.2021.126096>
- Van Yken, J.; Boxall, N.J.; Cheng, K.Y.; Nikoloski, A.N.; Moheimani, N.R.; Kaksonen, A.H.: E-waste recycling and resource recovery: a review on technologies, barriers and enablers with a focus on Oceania. *Metals* (2021). <https://doi.org/10.3390/met11081313>
- The Platinum Standard 2021. Heraeus Metal. (2021)
- Wang, M.; Tan, Q.; Chiang, J.F.; Li, J.: Recovery of rare and precious metals from urban mines—a review. *Front. Environ. Sci. Eng.* **11**, 1 (2017). <https://doi.org/10.1007/s11783-017-0963-1>
- Chang, Z.; Zeng, L.; Sun, C.; Zhao, P.; Wang, J.; Zhang, L., et al.: Adsorptive recovery of precious metals from aqueous solution using nanomaterials—a critical review. *Coord. Chem. Rev.* (2021). <https://doi.org/10.1016/j.ccr.2021.214072>
- González-García, P.: Activated carbon from lignocellulosics precursors: a review of the synthesis methods, characterization techniques and applications. *Renew. Sustain. Energy Rev.* **82**, 1393–1414 (2018). <https://doi.org/10.1016/j.rser.2017.04.117>
- Ismail, A.A.; Aroua, M.K.; Yusoff, R.: Palm shell activated carbon impregnated with task-specific ionic-liquids as a novel adsorbent for the removal of mercury from contaminated water. *Chem. Eng. J.* **225**, 306–314 (2013). <https://doi.org/10.1016/j.cej.2013.03.082>
- Yu, M.; Zeng, S.; Wang, Z.; Hu, Z.; Dong, H.; Nie, Y., et al.: Protic ionic-liquid-supported activated carbon with hierarchical pores for efficient NH<sub>3</sub> adsorption. *ACS Sustain. Chem. Eng.* **7**, 11769–11777 (2019). <https://doi.org/10.1021/acssuschemeng.9b02051>
- Abdul Rahim, A.R.; Mohsin, H.M.; Thanabalan, M.; Rabat, N.E.; Saman, N.; Mat, H., et al.: Effective carbonaceous desiccated coconut waste adsorbent for application of heavy metal uptakes by adsorption: equilibrium, kinetic and thermodynamics analysis. *Biomass Bioenergy* (2020). <https://doi.org/10.1016/j.biombioe.2020.105805>
- Kharrazi, S.M.; Mirghaffari, N.; Dastgerdi, M.M.; Soleimani, M.: A novel post-modification of powdered activated carbon prepared from lignocellulosic waste through thermal tension treatment to enhance the porosity and heavy metals adsorption. *Powder Technol.* **366**, 358–368 (2020). <https://doi.org/10.1016/j.powtec.2020.01.065>
- Macías-García, A.; Gómez Corzo, M.; Alfaro Domínguez, M.; Alexandre Franco, M.; Martínez, N.J.: Study of the adsorption and electroadsorption process of Cu (II) ions within thermally and chemically modified activated carbon. *J. Hazard. Mater.* **328**, 46–55 (2017). <https://doi.org/10.1016/j.jhazmat.2016.11.036>
- Lesaoana, M.; Mlaba, R.P.V.; Mtunzi, F.M.; Klink, M.J.; Ejidike, P.; Pakade, V.E.: Influence of inorganic acid modification on Cr(VI) adsorption performance and the physicochemical properties of activated carbon. *S. Afr. J. Chem. Eng.* **28**, 8–18 (2019). <https://doi.org/10.1016/j.sajce.2019.01.001>
- Nadeem, M.; Mahmood, A.; Shahid, S.A.; Shah, S.S.; Khalid, A.M.; McKay, G.: Sorption of lead from aqueous solution by chemically modified carbon adsorbents. *J. Hazard. Mater.* **138**, 604–613 (2006). <https://doi.org/10.1016/j.jhazmat.2006.05.098>
- Rehman, A.; Park, M.; Park, S.-J.: Current progress on the surface chemical modification of carbonaceous materials. *Coatings* **9**, 103 (2019). <https://doi.org/10.3390/coatings9020103>
- Fajar, A.T.N.; Hanada, T.; Goto, M.: Recovery of platinum group metals from a spent automotive catalyst using polymer inclusion membranes containing an ionic liquid carrier. *J. Membr. Sci.* **629**, 119296 (2021). <https://doi.org/10.1016/j.memsci.2021.119296>
- Paiva, A.: Recycling of palladium from spent catalysts using solvent extraction—some critical points. *Metals* **7**, 505 (2017). <https://doi.org/10.3390/met7110505>
- Abdelhamid, H.N.; Khan, M.S.; Wu, H.-F.: Design, characterization and applications of new ionic liquid matrices for multifunctional analysis of biomolecules: a novel strategy for pathogenic bacteria biosensing. *Anal. Chim. Acta* **823**, 51–60 (2014). <https://doi.org/10.1016/j.aca.2014.03.026>



21. Hospital-Benito, D.; Lemus, J.; Moya, C.; Santiago, R.; Palomar, J.: Process analysis overview of ionic liquids on CO<sub>2</sub> chemical capture. *Chem. Eng. J.* **390**, 124509 (2020). <https://doi.org/10.1016/j.cej.2020.124509>
22. Kang, T.; Park, Y.; Choi, K.; Lee, J.S.; Yi, J.: Ordered mesoporous silica (SBA-15) derivatized with imidazole-containing functionalities as a selective adsorbent of precious metal ions. Electronic supplementary information (ESI) available: TEM image of SBA-15. See <http://www.rsc.org/suppdata/jm/b3/b315829b/>. *J. Mater. Chem.* **14**:1043 (2004) doi:<https://doi.org/10.1039/b315829b>
23. Kumar, A.S.K.; Sharma, S.; Reddy, R.S.; Barathi, M.; Rajesh, N.: Comprehending the interaction between chitosan and ionic liquid for the adsorption of palladium. *Int. J. Biol. Macromol.* **72**, 633–639 (2015). <https://doi.org/10.1016/j.ijbiomac.2014.09.002>
24. Sharma, S.; Wu, C.M.; Koodali, R.T.; Rajesh, N.: An ionic liquid-mesoporous silica blend as a novel adsorbent for the adsorption and recovery of palladium ions, and its applications in continuous flow study and as an industrial catalyst. *RSC Adv.* **6**, 26668–26678 (2016). <https://doi.org/10.1039/c5ra26673d>
25. Zhang, X.; Wang, D.; Zhao, N.; Al-Arif, A.S.N.; Aouak, T.; Al-Othman, Z.A., et al.: Grafted ionic liquid: Catalyst for solventless cycloaddition of carbon dioxide and propylene oxide. *Catal. Commun.* **11**, 43–46 (2009). <https://doi.org/10.1016/j.catcom.2009.08.007>
26. Liévano, J.F.P.; Díaz, L.A.C.: Synthesis and characterization of 1-Methyl-3-Methoxysilyl propyl imidazolium chloride—mesoporous silica composite as adsorbent for dehydration in industrial processes. *Mater. Res.* **19**, 534–541 (2016). <https://doi.org/10.1590/1980-5373-MR-2015-0561>
27. Lin, Y.; Xu, H.; Gao, Y.; Zhang, X.: Preparation and characterization of hydrochar-derived activated carbon from glucose by hydrothermal carbonization. *Biomass Convers. Biorefinery* (2021). <https://doi.org/10.1007/s13399-021-01407-y>
28. Han, X.; Wang, Y.; Zhang, N.; Meng, J.; Li, Y.; Liang, J.: Facile synthesis of mesoporous silica derived from iron ore tailings for efficient adsorption of methylene blue. *Colloids Surf. A* **617**, 126391 (2021). <https://doi.org/10.1016/j.colsurfa.2021.126391>
29. Nguyen, T.T.; Duy Nguyen, T.H.; Thi Huynh, T.T.; Dinh Dang, M.H.; Thuy Nguyen, L.H.; Le Hoang, D.T., et al.: Ionic liquid-immobilized silica gel as a new sorbent for solid-phase extraction of heavy metal ions in water samples. *RSC Adv.* **12**, 19741–19750 (2022). <https://doi.org/10.1039/d2ra02980d>
30. Ahmed, A.; Chaker, Y.; Belarbi, E.H.; Abbas, O.; Chotard, J.N.; Abassi, H.B., et al.: XRD and ATR/FTIR investigations of various montmorillonite clays modified by monocationic and dicationic imidazolium ionic liquids. *J. Mol. Struct.* **1173**, 653–664 (2018). <https://doi.org/10.1016/j.molstruc.2018.07.039>
31. Fatihah, N.; Arifin, T.; Azira, N.; Zulkipli, N.; Yusof, N.; Fauzi Ismail, A., et al.: Preparation and characterization of APTES-functionalized graphene oxide for CO<sub>2</sub> adsorption. *J. Adv. Res. Fluid Mech. Thermal Sci. J. Homepage* **61**, 297–305 (2019)
32. Hasanzadeh, M.; Simchi, A.; Shahriyari, F.H.: Nanoporous composites of activated carbon-metal organic frameworks for organic dye adsorption: synthesis, adsorption mechanism and kinetics studies. *J. Ind. Eng. Chem.* **81**, 405–414 (2020). <https://doi.org/10.1016/j.jiec.2019.09.031>
33. Chen, X.; Hossain, M.F.; Duan, C.; Lu, J.; Tsang, Y.F.; Islam, M.S., et al.: Isotherm models for adsorption of heavy metals from water—a review. *Chemosphere* (2022). <https://doi.org/10.1016/j.chemosphere.2022.135545>
34. Fosso-Kankeu, E.; Mittal, H.; Waanders, F.; Ray, S.S.: Thermodynamic properties and adsorption behaviour of hydrogel nanocomposites for cadmium removal from mine effluents. *J. Ind. Eng. Chem.* **48**, 151–161 (2017). <https://doi.org/10.1016/j.jiec.2016.12.033>
35. Sahmoune, M.N.: Evaluation of thermodynamic parameters for adsorption of heavy metals by green adsorbents. *Environ. Chem. Lett.* **17**, 697–704 (2019). <https://doi.org/10.1007/s10311-018-00819-z>
36. Karmaker, S.; Sintaha, F.; Saha, T.K.: Kinetics, isotherm and thermodynamic studies of the adsorption of reactive red 239 dye from aqueous solution by chitosan 8B. *Adv. Biol. Chem.* **09**, 1–22 (2019). <https://doi.org/10.4236/abc.2019.91001>
37. Torrik, E.; Soleimani, M.; Ravanchi, M.T.: Application of kinetic models for heavy metal adsorption in the single and multicomponent adsorption system. *Int. J. Environ. Res.* **13**, 813–828 (2019). <https://doi.org/10.1007/s41742-019-00219-3>
38. Qiu, H.; Lv, L.; Pan, B.C.; Zhang, Q.J.; Zhang, W.M.; Zhang, Q.X.: Critical review in adsorption kinetic models. *J. Zhejiang Univ., Sci., A* **10**, 716–724 (2009). <https://doi.org/10.1631/jzus.A0820524>
39. Plazinski, W.; Rudzinski, W.: Kinetics of adsorption at solid/Solution interfaces controlled by intraparticle diffusion: a theoretical analysis. *J. Phys. Chem. C* **113**, 12495–12501 (2009). <https://doi.org/10.1021/jp902914z>
40. Wiecka, Z.; Rzelewska-Piekut, M.; Regel-Rosocka, M.: Recovery of platinum group metals from spent automotive converters by leaching with organic and inorganic acids and extraction with quaternary phosphonium salts. *Sep. Purif. Technol.* (2022). <https://doi.org/10.1016/j.seppur.2021.119933>
41. Lommelen, R.; Vander Hoogerstraete, T.; Onghena, B.; Billard, I.; Binnemans, K.: Model for metal extraction from chloride media with basic extractants: a coordination chemistry approach. *Inorg. Chem.* **58**, 12289–12301 (2019). <https://doi.org/10.1021/acs.inorgchem.9b01782>
42. Zhang, Y.; Feng, X.; Qian, L.; Luan, J.; Jin, B.: Separation of arsenic and extraction of zinc and copper from high-arsenic copper smelting dusts by alkali leaching followed by sulfuric acid leaching. *J. Environ. Chem. Eng.* **9**, 105997 (2021). <https://doi.org/10.1016/j.jece.2021.105997>
43. Majima, H.; Izaki, T.; Sanuki, S.: Reductive stripping of Fe(III)-loaded D2EHPA with the aqueous solutions containing sulfur dioxide. *Metall. Trans. B* **16**, 187–194 (1985). <https://doi.org/10.1007/BF02679710>
44. Xu, B.; Kong, W.; Li, Q.; Yang, Y.; Jiang, T.; Liu, X.: A review of thiosulfate leaching of gold: focus on thiosulfate consumption and gold recovery from pregnant solution. *Metals* **7**, 222 (2017). <https://doi.org/10.3390/met7060222>
45. Mohdee, V.; Parasuk, V.; Pancharoen, U.: Synergistic effect of Thiourea and HCl on Palladium (II) recovery: an investigation on chemical structures and thermodynamic stability via DFT. *Arab. J. Chem.* **14**, 103196 (2021). <https://doi.org/10.1016/j.arabjc.2021.103196>
46. Al-Radadi, N.S.: Facile one-step green synthesis of gold nanoparticles (AuNp) using licorice root extract: antimicrobial and anticancer study against HepG2 cell line. *Arab. J. Chem.* (2021). <https://doi.org/10.1016/j.arabjc.2020.102956>
47. Chen, B.; He, J.; Xi, Y.; Zeng, X.; Kaban, I.; Zhao, J., et al.: Liquid-liquid hierarchical separation and metal recycling of waste printed circuit boards. *J. Hazard. Mater.* **364**, 388–395 (2019). <https://doi.org/10.1016/j.jhazmat.2018.10.022>
48. Kasper, A.C.; Veit, H.M.: Gold recovery from printed circuit boards of mobile phones scraps using a leaching solution alternative to cyanide. *Braz. J. Chem. Eng.* **35**, 931–942 (2018). <https://doi.org/10.1590/0104-6632.20180353s20170291>
49. Kim, B.-S.; Lee, J.-C.; Jeong, J.; Yang, D.-H.; Shin, D.; Lee, K.-I.: A Novel process for extracting precious metals from spent mobile phone PCBs and automobile catalysts. *Mater. Trans.* **54**, 1045–1048 (2013). <https://doi.org/10.2320/matertrans.M2013051>
50. Gurung, M.; Adhikari, B.B.; Kawakita, H.; Ohto, K.; Inoue, K.; Alam, S.: Recovery of gold and silver from spent mobile phones by means of acidothiourea leaching followed by adsorption





- using biosorbent prepared from persimmon tannin. *Hydrometallurgy* **133**, 84–93 (2013). <https://doi.org/10.1016/j.hydromet.2012.12.003>
51. Ippolito, N.M.; Medici, F.; Pietrelli, L.; Piga, L.: Effect of acid leaching pre-treatment on gold extraction from printed circuit boards of spent mobile phones. *Materials* **14**, 362 (2021). <https://doi.org/10.3390/ma14020362>
52. Bui, T.H.; Jeon, S.; Lee, Y.: Facile recovery of gold from e-waste by integrating chlorate leaching and selective adsorption using chitosan-based bioadsorbent. *J. Environ. Chem. Eng.* **9**, 104661 (2021). <https://doi.org/10.1016/j.jece.2020.104661>
53. Zazycki, M.A.; Tanabe, E.H.; Bertuol, D.A.; Dotto, G.L.: Adsorption of valuable metals from leachates of mobile phone wastes using biopolymers and activated carbon. *J. Environ. Manage.* **188**, 18–25 (2017). <https://doi.org/10.1016/j.jenvman.2016.11.078>
54. Kubota, F.; Kono, R.; Yoshida, W.; Sharaf, M.; Kolev, S.D.; Goto, M.: Recovery of gold ions from discarded mobile phone leachate by solvent extraction and polymer inclusion membrane (PIM) based separation using an amic acid extractant. *Sep. Purif. Technol.* **214**, 156–161 (2019). <https://doi.org/10.1016/j.seppur.2018.04.031>
55. Zhou, W.; Liang, H.; Xu, H.: Recovery of gold from waste mobile phone circuit boards and synthesis of nanomaterials using emulsion liquid membrane. *J. Hazard. Mater.* **411**, 125011 (2021). <https://doi.org/10.1016/j.jhazmat.2020.125011>

